Dalton Transactions

Accepted Manuscript

This is an *Accepted Manuscript*, which has been through the Royal Society of Chemistry peer review process and has been accepted for publication.

Accepted Manuscripts are published online shortly after acceptance, before technical editing, formatting and proof reading. Using this free service, authors can make their results available to the community, in citable form, before we publish the edited article. We will replace this *Accepted Manuscript* with the edited and formatted *Advance Article* as soon as it is available.

You can find more information about *Accepted Manuscripts* in the Information for Authors.

Please note that technical editing may introduce minor changes to the text and/or graphics, which may alter content. The journal's standard Terms & Conditions and the Ethical guidelines still apply. In no event shall the Royal Society of Chemistry be held responsible for any errors or omissions in this *Accepted Manuscript* or any consequences arising from the use of any information it contains.

ROYAL SOCIETY OF CHEMISTRY

www.rsc.org/dalton

Dalton Transactions

RSCPublishing

ARTICLE

Enhanced photocatalytic activities of the heterostructured upconversion photocatalysts with cotton mediated on $TiO_2/ZnWO_4$:Yb^{3+}, Tm^{3+}

Cite this:

DOI: 10.1039/xoxxoooooox

Received ooth January 2012,
Accepted ooth January 2012

DOI: 10.1039/xoxxoooooox

www.rsc.org/

Kaili Feng, Shouqiang Huang, Ziyang Lou*, Nanwen Zhu and Haiping Yuan

To improve the photocatalytic efficiency and make full use of solar energy, $ZnWO_4$: Yb^{3+}, Tm^{3+} (ZYT) was introduced as the upconversion luminescence agent on TiO_2 with cotton template, and a novel upconversion photocatalysts of $TiO_2/ZnWO_4$: Yb^{3+}, Tm^{3+} (TZYT-C) were synthesized and optimized with 5%-30% of ZYT. The heterostructure between ZYT and TiO_2 was formed in the TZYT-C composites with the presence of tube-like morphologies due to the additive of cotton template. The UV (364 nm) and blue (484 nm) light were emitted from ZYT upon 980nm NIR irradiation. The BET specific surface areas of all the TZYT-C composites increased from 37 m^2/g (TiO_2-C) to the maximum value of 75 m^2/g on 5%TZYT-C. The photocatalytic activities of the TZYT-C composites were tested using the degradation process of methyl orange (MO). 5%TZYT-C showed the highest degradation efficiency, with a value of 55.6% under sun-like irradiation for 210 min. The same performance was observed on 5%TZYT-C under NIR ($\lambda \geq 780$nm)irradiation, with a maximum removal rate of 9.02%, since 5%TZYT-C showed the highest efficient electron-hole (e^-/h^+) pair separation, comparing to ZYT and other TZYT-C composites.

1 Introduction

Titanium dioxide (TiO_2) has been proven to be the most promising photocatalyst for organic pollution degradation, while only the UV light, 5% of the solar spectrum, could be absorbed and utilized. Several enhancement methods, such as the surface modification[1], organic/inorganic metal doping[2, 3] and the combination with narrow band gap semiconductors[4], have been applied and tested to extend the light absorption spectrum from UV to visible light. The conversion of long wavelength light to UV light is another promising way, which could extend the utilization of the sunlight energy, and improve the photocatalytic efficiency.

Upconversion illustrates anti-Stokes luminescence processes, which converts two or more low-energy pump photons to generate a higher-energy photon by continuous absorption or energy transfer.[5,6] Upconversion luminescence photocatalysts have been found to be an effective way to utilize the NIR light, with the aid of trivalent lanthanides (Ln^{3+}) ions, and converse the NIR light to UV and short-wavelength visible light.[7,8] Ln^{3+} ions exhibit remarkable optical properties by means of three types of energy transitions: inner configurational 4f-4f transition, inter configurational 5d-4f transition and charge transfer transition,[9-11] among which Yb^{3+} is one of the best sensitizer candidates due to its large absorption cross-section around 980nm.[12] In the process of photocatalytic degradation, Yb^{3+} ions can absorb the NIR light and transfer the energy to activators, i.e. Tm^{3+} and Er^{3+} ions.[13-15] Then the energy can be transferred to the host material, followed by an oxidative hole (h^+) generation by extraction of a reductive electron from a valence band of the semiconductor.

Tungstate family is one of the promising upconversion materials. Zinc tungstate ($ZnWO_4$) has proven to be good properties as scintillator crystal or phosphor,[16-17] and some other advantages benefited for upconversion, such as high chemical stability, high average refractive index, high X-ray absorption coefficient, high light yield, short decay time and low afterglow to luminescence.[18-19] The formation of heterostructure between two semiconductors will also improve the separation of e^-/h^+ pairs efficiently, and TiO_2 and $ZnWO_4$ are the two semiconductors candidates, to form the n-n type heterostructure.[20-22] Herein, TZYT semiconductors were synthesized, where ZYT is a n-type semiconductor upconversion agent and TiO_2 is a n-type semiconductor with efficient UV light photocatalytic activity.

The morphologies and the specific surface area of the photocatalysts will influence photocatalytic activities greatly, and tubulous structure is the suitable one to improve the photocatalysts performance. Some organic materials, such as cotton fiber[23-25], microalgae[26] and leaves[27] with natural structure, have been introduced and proven to be the suitable templates because of its economic, affordable and special structure. For example, TiO_2 hollow fiber materials are found to be a good choice for methylene blue (MB) degradation, as proved by Zheng et al[28]and Su et al[29]. Thus, cotton is chosen as the template for the upconversion photocatalysts preparation, to build the tubulous structure.

In this work, novel upconversion photocatalysts of the TZYT-C composites were synthesized by a simple sol-gel method. The TZYT-C composites were optimized by doping ZYT with various contents (5%, 10%, 20% and 30%), which assigned as 5%TZYT-C,

Dalton Transactions Accepted Manuscript

10%TZYT-C, 20%TZYT-C and 30%TZYT-C, respectively. The as-prepared samples were characterized by phase analysis, morphologies analysis, optical properties and upconversion luminescence. Further to these, the TZYT-C composites were assessed by the photocatalytic degradation of methyl orange (MO) under UV-vis-NIR and NIR light source conditions.

2 Experimental sections

2.1 Materials and methods

$ZnSO_4 \cdot 7H_2O$, $Yb(NO_3)_3 \cdot 5H_2O$, $Tm(NO_3)_3 \cdot 5H_2O$, $Na_2WO_4 \cdot 2H_2O$, Titanium isopropoxide (TTIP), anhydrous ethanol and methyl orange with analytical-grade were used for the photocatalysts' preparation. All of them and the medical defatted cotton were purchased from Sinopharm Chemical Reagent Co. Ltd (China). No further purification process was applied for these chemical compounds.

2.1.1 Synthesis of $ZnWO_4$ and ZYT products

$ZnSO_4 \cdot 7H_2O$ (8mmol) was added into 100mL deionized water, under the vigorous stirring. Meanwhile, $Na_2WO_4 \cdot 2H_2O$ (8mmol) was added into 100mL deionized water. Then the $ZnSO_4 \cdot 7H_2O$ solution was transferred into a three neck round bottom flask, with the Na_2WO_4 solution titration drop by drop under continuous stirring, and maintained at 80°C for 6h. Afterwards, the white precipitate was separated through centrifugation, and the precipitation should be washed with anhydrous ethanol solution for three times and dried at 60°C in a vacuum oven. When cooling down, the product was calcined at 500°C for 4h and then cooled down to room temperature. The same synthesis procedure for ZYT, except to the additive of $ZnSO_4 \cdot 7H_2O$ (8mmol), $Yb(NO_3)_3 \cdot 5H_2O$ (0.4mmol), $Tm(NO_3)_3 \cdot 5H_2O$ (0.04mmol) and $Na_2WO_4 \cdot 2H_2O$ (8mmol) in the first step.

2.1.2 Preparation of pure TiO_2 and TiO_2-C

Titanium isopropoxide (TTIP) (4mmol) was added into anhydrous ethanol (pH=1) drop by drop, and then at 80°C for 6h in the thermostat water bath. The white precipitation was separated by centrifugation for three times at 4000r/min, and then washed by anhydrous ethanol each time. The precipitation obtained was dried at 60°C in a vacuum oven until it was waterless, and then calcined at 500°C for 4h. TiO_2 was finally obtained after cooling down to room temperature. As for TiO_2-C, 1.2g cotton split was introduced into the mixed TTIP and anhydrous ethanol solution before thermostat water bath. The procedure followed was consistent with TiO_2 products.

2.1.3 Preparation of TZYT and TZYT-C samples

0.0160g、0.0319g、0.0639g、0.0958g ZYT powder prepared were introduced to 40mL distilled water according to the mass ratios of 5%, 10%, 20% and 30%, respectively. 1.2mL TTIP solution was added to 40 mL anhydrous ethanol, with a stirring rod stirring, and titrated into the ZYT solution drop by drop. In addition, 1.2g cotton split was introduced into the above solution for the preparation of the TZYT-C composites. The mixtures were kept in a thermostat water bath at 80°C for 6h. The process followed was consistent with ZYT powders.

2.2 Characterization

The X-ray diffraction (XRD) patterns of the samples were recorded by using Cu Kα X-radiation, at 40 kV and 30 mA using an X-ray diffractometer with a scan speed of 4° min^{-1}. The morphologies were characterized with JEM-2010HT transmission electron microscope (TEM) and Sirion 200 field emission scanning electron microscope (FESEM), which equipped with the Oxford ICA energy-dispersive spectroscopy (EDS) instrument. A Lambda 750 UV-vis-NIR (ultraviolet-visible-near-infrared) spectrophotometer was used to obtain the adsorption spectra, and then the formula $(\alpha h\upsilon)^{1/2}$ was used to calculate the band gap (E_g), in which α, h, υ reference to absorption coefficient, Planck's constant, light frequency, respectively. The N_2 adsorption-desorption isotherm was used to calculate the surface area and pore size distribution by the Brunauer–Emmett–Teller (BET) method and Barett–Joyer–Halenda (BJH), respectively. The photoluminescence (PL) spectra were recorded on a Hitachi F-7000 fluorescence spectrophotometer. Upconversion luminescence was tested by a 980nm semiconductor laser, which installed in the F-7000 fluorescence Spectrophotometer as an excitation light source.

2.3 Photocatalytic performance

MO was one of the most popular dyed organics, which used widely in testing photocatalytic activities. The ratio of the sample and MO aqueous solution was 1mg:1mL, and the initial concentration of MO aqueous solution was 10mg/L. The mixture solution kept stirring in the dark for 2h, and then irritated by the light source of Mercury lamp or Xenon lamp, which was used to simulate the UV light and sunlight, respectively. Near-infrared (NIR) and visible light conditions were simulated by the means of fixing optical filters. In the process of photocatalytic degradation, 0.03g as-synthesized products were added into 30mL MO solutions and 2mL samples were taken out at the defined internal times, and then centrifugated at 12000rpm for 5 min. The supernatant obtained was used to determine the MO content at 464nm wavelength, using a UV-3900 spectrophotometer. Finally, according to its relationship between absorbance and concentration, we could obtain the degradation efficiency.

2.4 Detection of hydroxyl radical （·OH）and superoxide radicals （$\cdot O_2^-$）

Terephthalic acid (TA, 4×10^{-4}M) was added into NaOH (2×10^{-3}M) solution and 20mg photocatalysts were mixed with 20 mL TA solution, respectively. The mixture solution kept stirring in the dark for 2h, and then irritated by the light source of Xenon lamp, which was used to simulate the sunlight. 0.03g as-synthesized products were added into 30mL MO solutions and 2mL samples were taken out at the defined internal times, and then centrifugated at 12000rpm for 5 min. The PL spectra of the 2-hydroxyterephthalic acid were recorded on a Hitachi F-7000 fluorescence spectrophotometer with an excitation wavelength of 320 nm, which could detect ·OH radicals. Nitroblue tetrazolium (NBT, 1×10^{-3}M) solutions was used to detect $\cdot O_2^-$ radical in the same way.

Dalton Transactions Accepted Manuscript

 This journal is © The Royal Society of Chemistry 2012

3 Results and Discussion

3.1 Crystal structure

Fig. 1 showed the XRD patterns of TiO_2-C, ZYT and 5%TZYT-C. TiO_2-C contained both anatase and rutile phases, and the diffraction peaks of $2\theta = 25.37°, 38.61°, 48.12°, 53.97°$ matched well with the (101), (112), (200), (105), (211) planes (JCPDS, card no. 84-1285), while the diffraction peaks of rutile were located at 27.48°, 36.13, 54.37° , matched well with the (110), (101), (211) planes (JCPDS, card no. 89-8301). The main diffraction peaks of ZYT were 23.79°, 24.47°, 30.50°, 36.34°, 38.10°, 41.17°, 48.69°, 50.15°, 51.83°, 53.66°, which were perfectly indexed to its (011), (110), (111), (021), (200), (102), (022), (220), (130), (202) planes (JCPDS, card no. 73-0554). After the combination of TiO_2-C and ZYT, the obtained 5%TZYT-C composite contained the anatase, rutile and $ZnWO_4$ phases simultaneously. As the contents of ZYT increased from 5% to 30% (Fig.S1), the diffraction peaks of anatase in the TZYT-C composites became weak and broaden, while the diffraction peak intensities of $ZnWO_4$ enhanced gradually.

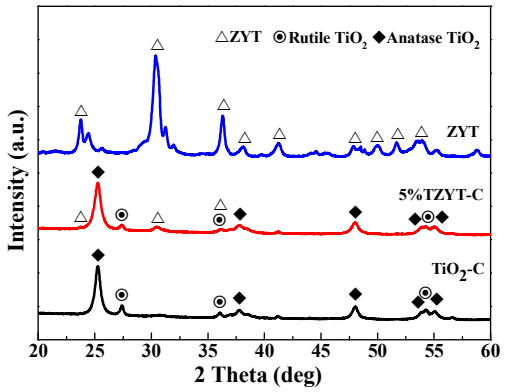

Fig.1 XRD patterns of TiO_2-C, ZYT, 5%TZYT-C.

According to the Scherrer formula,[30] the calculated grain size of anatase in 5%TZYT-C was 12.16 m, smaller than that of TiO_2-C (15.97 nm), indicating that with the increase of ZYT content, the average grain size of the overall particle became smaller, which will benefit for the photocatalyst performance through the increase of the contact areas with the substances.

3.2 Morphology analysis

The morphologies of the samples were investigated by SEM and TEM. The stripped morphology of the used raw cotton fibers with smooth surface was displayed (Fig. 2a and b), and thus the hollow tubular structure for the cotton templated TiO_2 samples could be formed after the pyrolysis at 500°C. As shown in Fig. 2d and g, 5%TZYT-C possesses the tube-like morphology. With the increment of ZYT content (Fig. 2e), the same morphology of 30%TZYT-C could also be maintained. The tubular structure of the TZYT-C composites were built with many nanoparticles (Fig. 2f), which included TiO_2 and $ZnWO_4$ (Fig. 2c) particle. The high-resolution TEM (HRTEM) image provided the lattice fringe spacing of 0.243 nm, with the corresponding distance of the (103) plane of anatase TiO_2. According to the Scherrer formula referred above, it had been

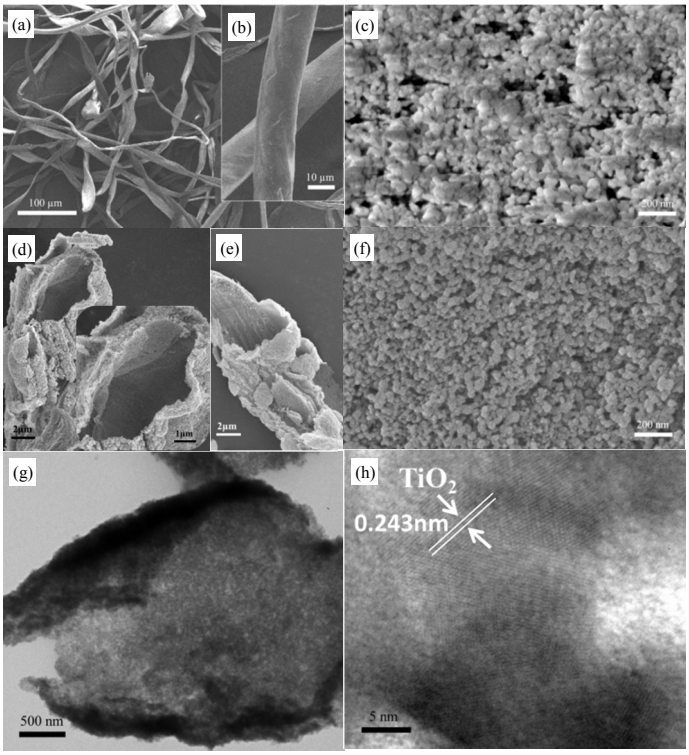

Fig.2 SEM images of (a, b) raw cotton and the as-prepared (c) ZYT, (d, f) The hollow tubular structure and surface of 5%TZYT-C (g) TEM and (h) HRTEM images of 5%TZYT-C.

verified that the synthesis decreased the grain size of the particles, which indicated that ZYT and TiO_2 integrated with each other and brought about smaller particles.

A novel form with a hollow structure could be found in Fig.2d and g. The formative shape was in the approach of the combination with cotton, which used as a template to form a hollow shape. It can take advantages over the striped cotton fiber, in order to enhance the surface area and further improve the contact with target pollutants including aqueous or atmospheric matters.

To verify the pore shape and pore size distribution of the samples, BET and BJH methods were used and displayed in Fig.3a and b, respectively. It showed that both of the nitrogen adsorption isotherms of TiO_2-C and 5%TZYT-C ascended slowly when they were in relative low P/P_0, and 5%TZYT-C became more slope than

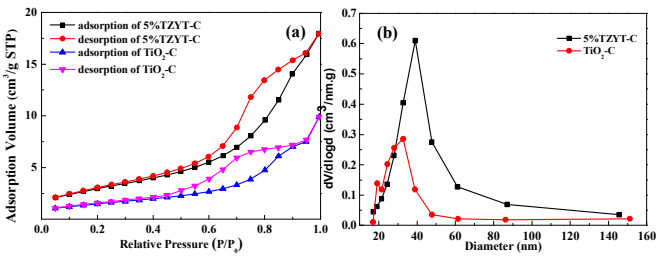

Fig.3 (a) Nitrogen adsorption-desorption isotherm of 5%TZYT-C and TiO_2-C and (b) BJH pore size distribution obtained from 5%TZYT-C and TiO_2-C.

Dalton Transactions Accepted Manuscript

TiO_2 with the increase of relative pressure. As shown in the plots, the nitrogen isotherm for 5%TZYT-C and TiO_2-C were IUPAC type III and type V, indicating that the adsorbent-adsorbate interactions played an important role and obtained with certain porous adsorbents. Obvious hysteresis loops could also be found in Fig.3a, which appearing in the multilayer range of physisorption isotherms was usually associated with capillary condensation in mesoporous structures. According to IUPAC, a type H1 hysteresis loop was found in 5%TZYT-C, indicating that the sample material was with relative narrow distribution of mesopore size and approximately uniform spheres agglomerated. By comparison, there existed more mesoporous structure than TiO_2-C. Furthermore, the desorption-adsorption curves also depicted a tubular cylinder with open ended, which was in great agreement with the tubulous hollow structure showed in SEM graphs. Fig.3b showed the BJH pore size distribution, and the result matched with the above characters, which concluded that the pore structure has changed since the introduction of ZYT.

BET surface areas of the samples were shown in Table 1. It could be seen that the surface area of pure TiO_2-C was 37 $m^2 g^{-1}$, the surface areas of TZYT-Cs were much higher than TiO_2-C and ZYT. 5%TZYT-C showed the highest degradation efficiency under the sun-like light, which had the surface area of 75 $m^2 g^{-1}$. The results of BET surface areas were in accordance with the calculated grain size. With the decrease of grain size, the TZYT-C composites obtained more surface areas, which enlarged the contact areas with other substances.

Table1. BET surface area of the samples.

Sample	ZYT	TiO_2-C	5%TZYT-C	10%TZYT-C	20%TZYT-C	30%TZYT-C
Surface Area(m^2/g)	13	37	75	66	69	73

3.3 UV-vis-NIR absorption properties

The UV-vis-NIR absorption spectra of the as-synthesized samples were shown in Fig.4. It could be observed that the absorption spectra from 5%TZYT-C to 30%TZYT-C were in uniform trace, possessed high absorbance in the UV light region. As shown in Fig.4a, ZYT sample showed lower absorbance than the TZYT-C composites under UV wavelength (λ≤380nm) conditions.

To verify the consequence of inverting ZYT, the band-gap energies of the samples were calculated according to the plots of $(\alpha h\nu)^{1/2}$ versus photon energy ($h\nu$),[31] where α referred to the absorption coefficient, h was the Planck's constant, ν was the frequency. As shown in Fig.4b, the plot showed us the band gaps of TiO_2-C and ZYT were 2.9eV and 3.8eV, respectively, while that of the TZYT-C composites were around 3eV. However, there were other absorption peaks in ZYT could be found, which due to the transitions of Tm^{3+} ions. These added absorption peaks could also exist in the TZYT-C composites, and it will improve the utilization efficiency of sunlight.

Though the introduction ZYT hardly made changes to the band gap of the TZYT-C composites, and the combination of TiO_2 and ZYT could not change much to the absorbance wavelength, it would benefit to improve the luminescence properties.

3.4 Upconversion luminescence properties.

The upconversion emission spectra of ZYT and the TZYT-C composites under 980nm NIR light excitation were shown in Fig.5. ZYT showed much stronger upconversion luminescence intensity than the TZYT-C composites under 980nm NIR excitation. It could also be found that the notable emissions of ZYT, including the blue (484 nm) and red (656 nm) light, which corresponded to the $^1G_4 \rightarrow {}^3H_6$ and $^1G_4 \rightarrow {}^3F_4$ transitions of Tm^{3+} ions, respectively. By comparison, ZYT showed better upconversion characterization, for it could emission higher photon energy when excited with lower photon energy. The TZYT-C composites didn't show obvious transformation, which happened because Yb^{3+} transfers the energy to Tm^{3+} when it was excited under 980 nm NIR irradiation, and then the energy was further transferred to semiconductors. However, when ZYT was synthesized with TiO_2, the energy was further transferred to TiO_2. Though TiO_2 itself exhibits no upconversion ability, it was depicted to display upconversion performance in Fig.5c. Therefore, it needed further researches to improve the

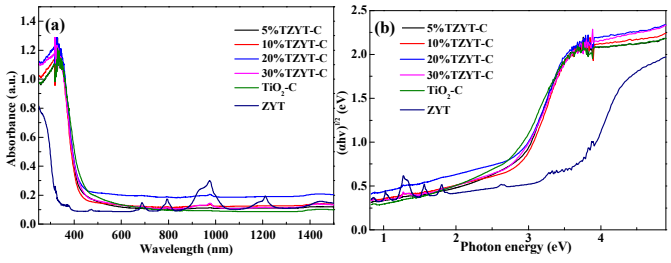

Fig.4 (a) The UV-vis-NIR Absorption spectra of the as-synthesized samples (b) The $(\alpha h\nu)^{1/2}$ – hν plot of the corresponding samples above.

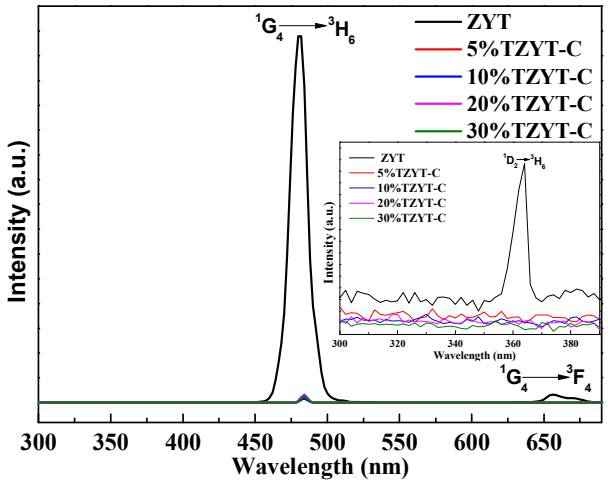

Fig.5 The upconversion emission spectra of the as-prepared samples under 980nm NIR excitation (2.5W).

Dalton Transactions Accepted Manuscript

This journal is © The Royal Society of Chemistry 2012

efficiency of energy transfer in the process. Actually, when it was in the 364nm wavelength, the samples showed weak peak which shown in the insert graph. It could be seen that the peak that irradiated in the range of UV light, corresponded to the $^1D_2 \rightarrow {}^3H_6$ transitions of Tm^{3+} ions, and it might be absorbed by ZYT, leading to the weak peak performance.

3.5 Degradation activities

The photocatalytic activities of the as-prepared composites were tested by the degradation of MO under sun-like light irradiation. As shown in Fig.6a, 5%TZYT-C displayed the most efficient degradation efficiency, with a value of 55.6% in 210min, higher than those of other TZYT-C composites. This may related to the heterostructure between TiO_2 and ZYT, which would be easier for the transfer of carrier and inhibited the recombination of e^-/h^+ pairs. The cotton template could also benefit for the degradation process of MO, since the formation of tubulous structure could increase the contact area, as shown in SEM and BET surface areas.

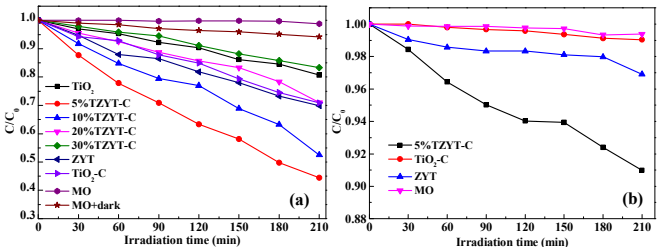

Fig.6 (a) The photocatalytic degradation of MO under sun-like light and (b) NIR ($\lambda \geq 780$nm) light irradiations.

On the other hand, Fig.6b displayed the photocatalytic degradation of the as-prepared samples under NIR spectrum. Obviously, it could figure out that 5%TZYT-C still showed much higher degradation efficiency than the other as-prepared samples, with the removal rate of 9.02%, much higher than that of TiO_2-C. The TZYT-C composites showed higher degradation efficiency in both conditions due to their special structure of heterostructure. Therefore, both the formation of heterostructure and the cotton template contributed to the improvement of MO degradation in 5%TZYT-C composite.

3.6 Degradation mechanism

Lanthanide ions (Ln^{3+}) co-doped into host materials could enhance the upconversion intensity when it was the combination of activator and sensitizer. The process was closely related to the energy transfer mechanism. On the basis of anti-stokes principle, it mainly had three luminescence theories containing excited state absorbance (ESA), energy transfer upconversion (ETU) and photon avalanche (PA). The most important mechanism between Yb^{3+} and Tm^{3+} was attributed to ETU according to the research studies. [32-33]

Among all the RE ions, Tm^{3+} ions was selected to be the activator in terms of its wealthy of ladder-like energy levels, which facilitated the photon absorption and energy transfer.[34] Meanwhile, Yb^{3+} ions, always co-doped with Tm^{3+} ions as the excellent sensitizers due to its large absorption cross-section near 980nm.[35]

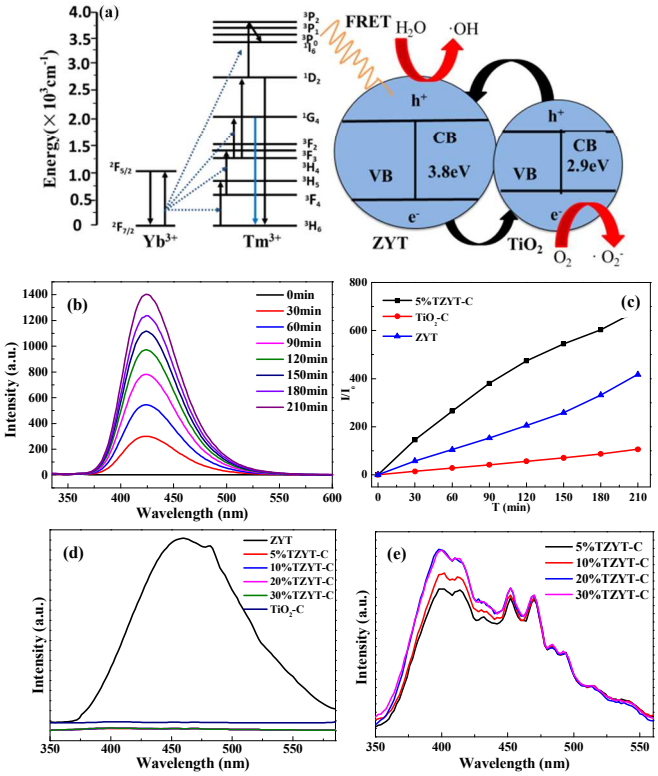

Fig.7 (a) The energy transfer Schematic illustration of TZYT composite under semiconductor laser irradiation (b) Time-dependent fluorescence spectra of the TA solution containing 20mg of 5%TZYT-C under sun-like light irradiation (c) The amount comparison of generated ·OH (d) The photoluminescence spectra intensity of TiO_2-C and the as-prepared products (e) The photoluminescence intensity comparison of the ZTYT-C composites.

As can be seen in Fig.7a, it clearly showed the sensitizers of Yb^{3+} ions and the formation of the excited states of Tm^{3+} ions, then as well as the activation of semiconductors and energy transferred between semiconductors. When irradiated under the 980nm NIR, Yb^{3+} ion was excited and came up with a transition from $^2F_{7/2}$ level to $^2F_{5/2}$ level. Then $^1G_4$, $^3F_2$ and $^3H_5$ levels of Tm^{3+} were populated by three sequential energy transfers from Yb^{3+} ions. Due to the large energy mismatch (about 3.5×10^3cm), the photon from Yb^{3+} ions couldn't populate the $^1D_2$ level of Tm^{3+} to transfer to $^1G_4$ level. The problem was probably related to the cross-relaxation between Tm^{3+} ions. Generally, there were two main forms to populate the $^1D_2$ level: one was $^3F_2 + {}^3H_4 \text{---} {}^3H_6 + {}^1D_2$ and $^1G_4 + {}^3H_4 \text{---} {}^3F_4 + {}^1D_2$, another was $^1D_2$ obtained the opportunity to transit to $^3P_2$ by the energy transfer of excited Yb^{3+}, then transferred to $^3P_1$ level through nonradioactively relax on the basis of Guo's [36] study.

The energy transferred from the RE ions to ZYT/TiO_2 semiconductors via fluorescence resonance energy transfer (FRET).[37] Then, activated ZYT and TiO_2 generate electrons and holes, as the oxidation and reduction agents, and heterostructure between ZYT and TiO_2 could be helpful for the transfer process. The electrons and holes in the inner ZYT and TiO_2 would shift to the surface and take part in the surface reaction. According to Mulliken electronegativity theory[20,38], the conduction band (CB) and valence

Dalton Transactions Accepted Manuscript

band (VB) position for ZYT and TiO_2 could be calculated by the equation of $E_{VB} = X - E^e + 0.5E_g$, $E_{CB} = E_{VB} - E_g$. The VB values and CB values for ZYT were 3.58 and -0.22, while those of TiO_2 were 2.76 and -0.14, respectively. Because the CB position of ZYT was higher than that of TiO_2, which lead to the electrons shift to TiO_2. The E_{VB} value of ZYT was larger than that of TiO_2, the holes can directly move to ZYT. Thus, photo-generated electrons and holes could separate efficiently. It was worthy pointing out that the photocatalytic abilities depended on the separation of electrons and holes. To restrain the recombination of electrons and holes could help to improve the photocatalytic performance.

The photo-generated electrons on the surface of TiO_2 would react with oxygen inner them to produce superoxide radical anions ($\cdot O_2^-$) or oxygen anions (O^{2-}) , since $\cdot O_2^-$ could interact with H^+ to form hydrogen peroxide (H_2O_2), furthermore, H_2O_2 can combine with $\cdot O_2^-$ to generate hydroxyl radical (·OH). ·OH had strong oxidizing properties and it could react with MO to degrade it into small molecule inorganic. The generation of ·OH on the surface of the TZYT-C composites could be detected by the PL technique using TA as a probe molecule.[39] According to the PL spectra of 2-hydroxyterephthalic acid at about 420nm showed in Fig.7b, ·OH indeed existed in the degradation process. And from Fig. 7c, it could be found that 5%TZYT-C composite generated much more amounts of ·OH than pure ZYT and TiO_2-C, which confirmed by the degradation results. Seeing Fig. S3a and b, it could be proved that the addition of ZYT could improve the photocatalytic degradation under NIR ($\lambda \geq 780$nm) light, in which there existed generated ·OH and $\cdot O_2^-$. The mechanism could be depicted in formulas [40, 41] below:

$$TZYT\text{-}C + h\nu \longrightarrow e_{CB}^- + h_{VB}^+ \quad (1)$$
$$h_{VB}^+ + H_2O \longrightarrow H^+ + \cdot OH \quad (2)$$
$$e_{CB}^- + O_2 \longrightarrow \cdot O_2^- \quad (3)$$
$$\cdot O_2^- + H^+ \longrightarrow HO_2\cdot \quad (4)$$
$$2HO_2\cdot \longrightarrow O_2 + H_2O_2 \quad (5)$$
$$HO_2\cdot + e_{CB}^- + H^+ \longrightarrow H_2O_2 \quad (6)$$
$$H_2O_2 + e_{CB}^- \longrightarrow OH^- + \cdot OH \quad (7)$$
$$H_2O_2 + \cdot O_2^- \longrightarrow O_2 + OH^- + \cdot OH \quad (8)$$
$$MO + \cdot OH \longrightarrow \text{degradation products} \quad (9)$$

As can be seen in Fig.7d, the emission intensity of PL spectrum depicted the variation between ZYT and the TZYT-C composites. The TZYT-C composites showed weak emission intensity in all spectra, and TiO_2-C and ZYT displayed stronger emission intensity in series. The recombination of photogenerated e^-/h^+ pairs, resulted in a higher emission peak, as showed in ZYT. The photo-generated e^-/h^+ pairs recombinated quickly, which could be concluded from the high peak of ZYT. It can't be absorbed because of the combination of e^-/h^+ pairs. However, when combined with TiO_2-C, the products showed lower intensity because the synthesis of ZYT and TiO_2 restrain the recombination of e^-/h^+ pairs. It could be found out that with the content of ZYT increased in Fig.7e, it has a growing peak in the UV light and visible light, meaning that the re-combination process enhances with more ZYT amounts added. All the TZYT-C composites had almost the same trend, as the wavelength increased from 450nm. Therefore, the heterostructure was designed here between ZYT and TiO_2 to restrain the recombination of certain e^-/h^+ pairs by transferring electrons from one semiconductor to other semiconductor efficiently.[22]

4 Conclusions

A novel NIR-driven TZYT-C heterostructure material with enhanced upconversion properties was prepared and 5%TZYT-C was found to be the best one for the MO degradation due to the larger surface area. The consequence of upconversion luminescence demonstrated that co-doping Yb^{3+} and Tm^{3+} ions into the new materials could improve the emission intensities, especially in UV(364nm) light and blue (484nm) light under NIR ($\lambda \geq 780$nm) radiation. The photocatalytic degradation activities showed that around 55.6 % and 9.02% of MO degradation efficiency were obtained under full spectrum of sun-like light and NIR spectrum conditions within 210 min, respectively. It was closely relative to the n-n type heterostructure between ZYT and TiO_2, which could also enhance the e^-/h^+ pair separation in the TZYT-C composites, and higher specific surface areas structure were obtained with the introduction of cotton template.

Acknowledgements

This work was financially supported by Shanghai Rising-Star Program (14QA1402400), National Natural Science Foundation of China (No. 51178350), Key project of Science and Technology Commission of Shanghai Municipality (No. 13DZ0511600), and National Key Technology R&D Program (No.2014BAL02B03-4).

Notes and references

[a]*School of Environmental Science and Engineering, Shanghai Jiao Tong University, Shanghai 200240, P. R. China*
Phone: +86 21 54743710; Fax number: +86 21 54743710
E-mail:louworld@126.com

1 L. W. Zhang, H. B. Fu and Y. F. Zhu, *Adv. Funct. Mater.,* 2008,18, 1.
2 X. H. Wang, J. G. Li, H. Kamiyama, Y. Moriyoshi and T. Ishigaki, *J. Phys. Chem. B,* 2006, 110, 6804.
3 G. Liu, Y. Zhao, C. Sun, F. Li, G. Q. Lu and H. M. Cheng, *Angew. Chem., Int. Ed.*, 2008, 47, 4516.
4 Y. Bessekhouad, N. Chaoui and M. Trzpit et al, *J. Photochem. Photobiol.*, A, 2006, 183, 218.
5 G. Chen, C. Yang and P. N. Prasad, *Acc. Chem. Res.*, 2013, 10,1021.
6 F. Auzel, *Chem. Rev.*, 2004, 104, 139–173.
7 Y. N. Tang, W. H. Di and X. S. Zhai, *ACS Catal.*, 2013,3, 405–412.
8 W.P. Qin, D. S. Zhang and D. Zhao et al, *Chem. Commun.*, 2010, 46, 2304–2306.
9 J. R. Lakowicz, Principles of Fluorescence Spectroscopy, Springer, Singapore, 2002.
10 O. S. Woleis, Lanthanide Luminescence, Springer, New York, 2011.
11 B. G. Wybourne, Optical Spectroscopy of Lanthanides, CRC Press, Taylor and Francis, Boca Raton, USA, 2007.
12 Q. Liu, W. Feng, F.Y. Li, *Coordin. Chem. Rev*, 2014, 273–274 ,100–110.
13 M. Haase, H. Sch¨afer, *Angew. Chem., Int. Ed.*, 2011, 50, 5808.
14 L. F. Liang, X. M. Zhang and H. L. Hu, *Mater. Lett.*, 2005, 59, 2186.
15 C. H. Li, F. Wang, J. Zhua and J. C. Yu, *Appl. Catal., B*, 2010, 100, 433.
16 V. Nagirnyi, E. Feldbach and L. Jonsson, *Nucl. Instrum. Methods Phys. Res., Sect. A,* 2002, 486, 395–398.
17 X. P. Chen, F. Xiao and S. Ye, *J. Alloys Compd.*, 2011, 509, 1355–1359.
18 J. S. Shi, L. L. Wang and Q. L. Wang, *J. Mater. Chem.C*, 2013, 1, 8033–8040.
19 M. Bonanni, L. Spanhel, M. Lerch, E. Fuglein and G. Muller, *Chem. Mater.*, 1998, 10, 304.
20 S.Q. Huang, Y.M. Feng, L.H.Han, *Adv.,* 2014, 4, 61679–61686 |
21 Y. L. Tian, B.B. Chang, J. L. Lu, *Appl. Mater. Interfaces*, 2013, 5, 7079−7085
22 Y. J. Hwang, A. Boukai, and P. D. Yang, *Nano Lett.*, 2009,9, 410-415.
23 X. Y. Tao, J. Du, Y.C. Yang, *Cryst. Growth Des.* ,2011, 11, 4422–4426.
24 S. Afzal, W.A. Daoud and S.J. Langford, *ACS Appl. Mater. Interfaces*,2013, 5, 4753−4759
25 M. Zhukovskyi, L. Sanchez-Botero and P. Matthew, *ACS Appl. Mater. Interfaces*, 2014, 6, 2262−2269
26 X.Y. Tao, R. Wu and Y. Xia, *ACS Appl. Mater. Interfaces*, 2014, 6, 3696−3702.

Dalton Transactions Accepted Manuscript

This journal is © The Royal Society of Chemistry 2012

27 X. F. Li, T. X. Fan and H. Zhou, *Advanced Adv. Funct. Mater*, 2009,19,1,45-56.
28 T. Zheng, Z. Tian, B. T. Su,et al. *Ind. Eng. Chem. Res.* 2012, 51, 1391–1395.
29 B.T.Su, K.Wang, N. Dong et al, *J. Mater. Process. Tech,* 2009, 209, 4088–4092.
30 L. L. Wang, Y. Y. Ma, H. Y. Jiang, *J. Mater. Chem. C*, 2014, 2, 4651–4658.
31 S. Q. Huang, N.W. Zhu and Z.Y. Lou, *Nanoscale*, 2014,6, 1362-1368.
32 X. Y. Huang, S. Y. Han, W. Huang and X. G. Liu, *Chem. Soc. Rev.*, 2013, 42, 173–201.
33 Y. Liu, D. Tu, H. Zhu, E. Ma and X. Chen, *Nanoscale*, 2013, 5, 1369–1384.
34 J. Zhou, Z. Liu and F. Y. Li, *Chem. Soc. Rev.*, 2012, 41, 1323–1349.
35 K. Z. Zheng, D. S. Zhang, D. Zhao, N. Liu, F. Shi and W. P. Qin, *Phys. Chem.*, 2010, 12, 7620–7625.
36 X. Y. Guo, W.Y. Song and C. F. Chen, *Phys.Chem. Chem. Phys.*, 2013, 15, 14681-14688.
37 Y. S. Liu, D. T. Tu and H. M. Zhu, *Adv. Mater.*, 2010, 22, 3266–3271.
38 J. Jiang, X. Zhang, P. B. Sun and L. Z. Zhang, *J. Phys. Chem. C*, 2011, 115, 20555–20564.
39 Y. N. Tang, W. H. Di, X. S. Zhai, R. Y. Yang and W. P. Qin, *ACS Catal.*, 2013, 3, 405.
40 C.C. Chen, X. Z. Li and W. h. Ma et al, *J. Phys. Chem. B* 2002, 106, 318-324.
41 C.C.Chen, W. Zh and Hisao. Hidaka et al, *Environ. Sci. Technol.* 2002, 36, 3604-3611

Dalton Transactions Accepted Manuscript